

## Obtaining equivalent fracture toughness of concrete using uniaxial compression test

Zongjin Li\*<sup>1</sup> and Yanhua Zhao<sup>2</sup>

<sup>1</sup>Department of Civil and Environmental Engineering, HongKong University of Science & Technology, Hong Kong, China  
<sup>2</sup>Department of Civil Engineering, Dalian University of Technology, Dalian, China

(Received October 12, 2009, Accepted January 21, 2010)

**Abstract.** From typical stress-axial strain curve and stress-volume strain curve of a concrete under uniaxial compression, the initiation and localization of microcracks within the interior of the specimen can be identified. The occurrence of random microcrack indicates the end of the linear elasticity, and the localization of microcrack implies formation of major crack, which triggers the onset of unstable crack propagation. The interval between initiation and localization of microcracks is characterized by a stable microcrack growth. Based on fracture behavior observed from a uniaxial compressive test of a concrete cylinder, a model has been developed to extract fundamental fracture properties of a concrete, i.e. the equivalent fracture toughness and the size of fracture process zone. The introduction of cracking Poisson's ratio accounts for tensile failure characteristics of concrete even under uniaxial compression. To justify the validity of the model proposed, tests on three-point bending have been performed to obtain the fracture toughness in accordance with two parameter fracture model and double-K fracture model. Surprisingly, it yields favorably comparable results and provides an encouraging alternative approach to determine fracture properties for concretes.

**Keywords:** concrete, microcrack, stress-strain relation, fracture toughness, uniaxial compression.

---

### 1. Introduction

It is well recognized that the failure of concrete is closely associated with microcrack development particularly at the weak interface between the cement paste and aggregates. Due to the sizeable microcrack development in fracture process zone, linear elastic fracture can not be directly applied to concrete. To account for then influence of the sizeable microcracks, a concept of effective quasi-brittle crack had been made to establish proper fracture model for concrete-like quasibrittle materials. When a concrete structure with the effective quasi-brittle crack is subjected to loading, the applied load will result, at certain level, in an energy release rate  $G$  at the tip of the effective quasi-brittle crack. The energy release rate  $G$  is composed by two portions: (i) the energy release rate in creating two surfaces generated by remote stress during specimen loading (the material surface energy), and (ii) the energy release rate in overcoming the local cohesive pressure,  $\sigma(w)$  during the separating the new surfaces. As a result, the total energy release rate,  $G_{II}$  for a mode I quasi-brittle crack can be expressed as

---

\* Corresponding author, Professor Zongjin Li, E-mail: [zongjin@ust.hk](mailto:zongjin@ust.hk)

$$G_{It} = G_{I\sigma} + G_{\sigma(w)} = G_{I\sigma} + \int_0^{CTOD} \sigma(w) dw \quad (1)$$

where  $G_{Ic}$  is the strain energy rate to create two new crack surfaces due to remote stress for mode I crack,  $\sigma(w)$  is the normal traction pressure which is the function of crack opening displacement  $w$  as explained earlier, and CTOD is the crack tip opening displacement. The crack shape is assumed to be a line. The two terms in the equation represent two types of energy dissipation mechanisms for fracture process have been introduced in the equation. The Griffith-Irwin energy dissipation mechanism is represented by a non-zero stress intensity factor and the Dugdale-Barenblatt energy dissipation mechanism is represented by the traction term. It seems that it is proper to use these two energy dissipation mechanism to describe the propagation of a quasi-brittle crack. However, one may approximately use models only based on a single fracture energy dissipation mechanism, either Griffith-Irwin energy dissipation mechanism by assuming  $\sigma(w)=0$  or the Dugdale-Barenblatt energy dissipation mechanism by assuming  $K_I=0$  to simplify the mathematical derivation. Based on different energy dissipation mechanism used, nonlinear fracture mechanics models for quasi-brittle materials may be classified as a fictitious crack approach and an equivalent-elastic crack approach (or an effective-elastic crack approach). Fracture models only using the Dugdale-Barenblatt energy dissipation mechanism are usually referred to as the fictitious crack approach, whereas fracture models using only the Griffith-Irwin energy dissipation mechanism are usually referred to as the effective-elastic crack approach.

In the category of fictitious crack approach, Hillerborg *et al.* (1976a, 1985b) have proposed a cohesive model with  $K_I=0$ . Recently, Asferg *et al.* (2007) developed an extended finite element (XFEM) scheme for modeling of cohesive crack growth. Bazant and Oh (1983) have developed a crack band model using similar concept. In the category of effective-elastic crack approach, two representative models are the two-parameter fracture model (TPFM) by Shah and Jenq (1985a, 1985b) and the size effect model (SEM) by Bazant and Kazemi (1990). Moreover, the double- $K$  model (DKM) has been developed by Xu (1998). It has been used to study the energy dissipation along fracture process zone in concrete by Zhao *et al.* (2003). Dujc *et al.* (2010) have developed a quadrilateral finite element model for tensile fracture of an embedded crack in a 2-D concrete. In effective-elastic crack models, instead of original crack length, an effective-elastic crack length is used. The equivalence between the actual and the corresponding effective crack can be prescribed explicitly.

Most of the fracture parameters introduced in these models have to be experimentally evaluated. In TPFM, the critical stress intensity factor  $K_{Ic}^s$  and the critical crack tip opening displacement  $CTOD_c$  are determined by one size three-point bending beam through loading-unloading-reloading process (RILEM 1990). The same geometry is also recommended to determine the double- $K$  fracture parameters. In addition to the above mentioned three-point bending beam specimen, compact tension, wedge splitting and some other geometrical types of specimens are also used in these days to determine the fracture toughness of concretes. Even the Brazilian or splitting test but with an artificially induced notch in the tensile stress field has been used to measure the fracture toughness (Rasco 1987). Thus the coming questions may deserve our attentions: most of these specimens are pre-notched, i.e. exterior crack are introduced thath are somehow inconsistent with true conditions in the interior of a mass of concrete. Also the technique of preparing pre-notch may influence the response of the specimen and thus has to be carefully selected. Apart from these, those conventional methods require a quite delicate control during experiments. It is therefore worth to develop a new method with practically unnotched simply shaped specimen and easily controlled test.

The most common and basic test for concrete is the standard compression test, which can provide valuable information regarding characterization of concrete mechanical properties. Nevertheless little effort has been made to extract fundamental fracture properties from a uniaxial concrete compression test just because its failure behaviors do not directly relate to Mode I fracture. Studies conducted on concrete compression in 1960s observed the propagation of internal cracks with the help of various measuring techniques, such as x-ray photograph, microscope or laser holography (Shah 1968). Some experimental observations based on laser holography have shown crack path near the peak load are basically in the same direction as the applied load (Shah 1995). In reality, fracture of concrete under uniaxial compression can be easily observed for specimen with higher length to diameter ratio (Neville 2002). It is believed that failure in compression in these specimens is governed by the tensile property similar to that in splitting tension (Yin 1983, Su *et al.* 1988; Yin 1989). Or it can be put in this way: the failure of concrete under uniaxial compression is essentially manifestation of tensile cracking. The fracture mechanics can also be employed to describe the failure for concrete under uniaxial compression that has been confirmed by experimental results (Van Mier 1986). It should be indicated that the failure mode of a cylinder under compression is also influenced by the length and end condition of the platen (see Jansen *et al.* 1995, van Mier 1997, Choi and Shah 1998, and Carpeteri *et al.* 1999). The brittle failure induced by compression has been discussed in details by Horii and Nemat-Nasser (Horii and Nemat-Nasser 1986) has modeled the transition from brittle failure to ductile flow under very high confining pressures, by considering possible zone of plastically deformed materials at high shear-stress region around preexisting flaws. If the test conditions including the end condition and size of specimen can be well controlled, it should be able to predict the fracture behavior of concrete using the unnotched cylinder concrete specimen under uniaxial compression test by correlating the fracture properties of concrete with stress data, which is simpler than other methods.

In the present paper, an attempt has been made to obtain, through uniaxial compressive concrete test with unnotched cylinder, the equivalent fracture toughness. The apparent critical value as determined by our experiment is designated  $K_{IC}^C$  where superscript  $C$  is used to differentiate from its counterpart from previous studies. To gain the expression for  $K_{IC}^C$ , the basic concept of linear elastic fracture mechanics (LEFM) together with the interpretation of Poisson's ratio has been employed. To validate this method, the comparison has been made between the  $K_{IC}^C$  values from uniaxial compression test experiments and those from conventional method on the three-point bending beams of the concrete with same composition. It is found that the  $K_{IC}^C$  values are very close to the values obtained from the traditional methods.

## 2. Fracture behavior of concrete under uniaxial compression specimen

The fracture behavior of concrete is characterized by the formation and propagation of microcracks within the specimens. Based on microcrack development, the fracture process of a concrete under uniaxial compression can be divided into three stages: the random occurrence of microcracks, the stable extension (or the accumulation of microcracks) and failure with distinguished vertical crack. This can be distinguished in a typical stress-axial strain relationship as indicated in Fig. 1 (for ascending branch only), together with corresponding volumetric strain at various loading levels. The main symbols stand for:

$\sigma$  compressive stress

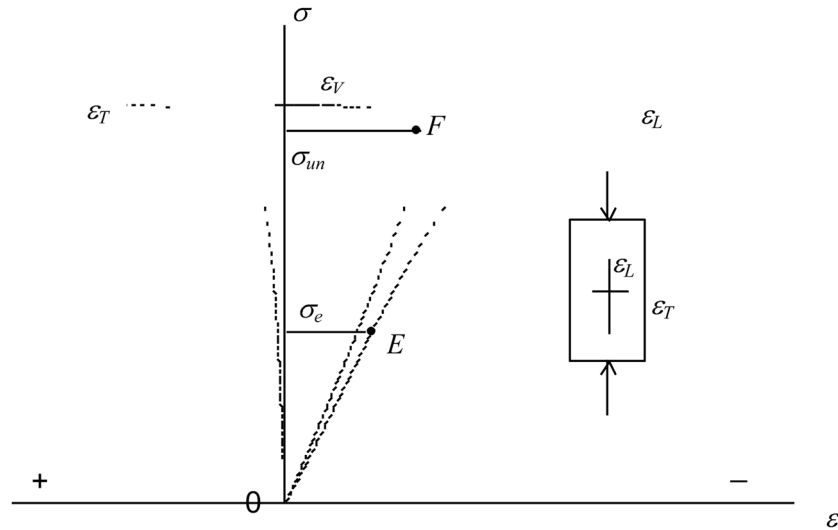


Fig. 1 The longitudinal and transversal deformation as well as volume profile for concrete cylinder under uniaxial compression

- $\epsilon_L$  longitudinal strain
- $\epsilon_T$  transversal strain
- $\epsilon_V = V/V_0 = \epsilon_L + 2\epsilon_T$  volumetric strain ( $\epsilon_L < 0, \epsilon_T > 0$ )

According to our model, referring to Fig. 1, microcracks occurring randomly starts from point *E* on the stress-axial strain curve. From the original point *O* to *E*, the material behaviors linearly elastic and no distinct microcracks occur due to loading. The volumetric deformation is also linearly elastic against the stress level. From the point *E* with stress level  $\sigma_e$ , the  $\sigma$ - $\epsilon$  curve deviates its straight path and this non-linearity may be attributed to the steady development of microcracks. During this process, according to our model, the pervasive internal cracks within the body may extend at the interface aggregate-matrix or in matrix in a stable manner up to the stress level  $\sigma_{un}$  (approximately above 90% of peak stress) corresponding the point *F* on the  $\sigma$ - $\epsilon_v$  curve. The critical discontinuity point *B F* poses significant importance because beyond this bound the volumetric strain  $\epsilon_v$  starts to increase rather than continuing to contract. It implies an instable development of a tension crack along vertical direction. This turnover point is clearly visible, and thus can be used to mark the proliferation and propagation of crack system in an unstable manner. At this very point, the stress intensity reaches its the critical level, and often the stress level at point *F* is sometimes related to the long-term strength of the concrete. Beyond this point *F*, the  $\sigma$ - $\epsilon_L$  curve bends over at an even increasing rate until the attainment of the ultimate stress  $\sigma_1$  within a rather short load.

The volume for cylinder is  $V=AH$ , where *A* and *H* are the bottom area and the height of the cylinder. When relating the area *A* with the perimeter *C*, we have  $V=C^2H/(4\pi)$ , that means the dependent variable *V* is a function of the independent variables *C* and *H*. In this case, the total derivative *dV* can be written as

$$dV = \frac{\partial V}{\partial C}dC + \frac{\partial V}{\partial H}dH = \frac{2C}{4\pi}HdC + \frac{C^2}{4\pi}dH \tag{2}$$

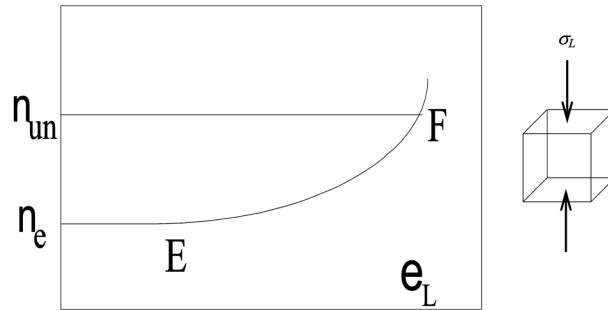


Fig. 2 The Poisson's ratio curve in uniaxial compression

When Eq. (2) is divided by  $V$  on both sides of, we have

$$\varepsilon_V = 2\varepsilon_c + \varepsilon_H \quad (3)$$

So the change in cylinder volume is composed of deformation change in circumference and height. Based on experimental observations, it is believed that the energy dissipation process prior the peak is dominated by global continuum process (Lee *et al.* 1997). To account for this global effect, the Poisson's ratio herein is determined by the ratio between the global transversal strain  $\varepsilon_C$  with respect to circumferential deformation and the corresponding longitudinal strain  $\varepsilon_H$  which can be formulated as

$$\nu = -\frac{\varepsilon_C}{\varepsilon_H} \quad (4)$$

For ordinary engineering materials, Eq. (4) produce a positive value  $\nu$  because of the opposite sign of  $\varepsilon_C$  and  $\varepsilon_H$ . For an isotropic and linear elastic material, it is constant. However for concrete, which is composed of several phases, it varies along with the longitudinal strain level as shown in Fig. 2. When the stress level is below elastic point  $E$ , the value of  $\nu$  can be regarded as a constant value and this value is just what we normally call the elastic Poisson's ratio. After point  $E$ ,  $\nu$  begins to increase at a higher rate until the peak stress. The value of  $\nu$  at the onset of initial microcracking and the unstable extension of microcracking are marked by the notation  $\nu_e$  and  $\nu_{un}$  respectively. The discrepancy between these two quantities is

$$\nu_{cr} = \nu_{un} - \nu_e \quad (5)$$

here a new name was assigned to  $\nu_{cr}$ : cracking Poisson's ratio. With this new item, the transverse deformation can be resolved into two parts: the first one is the strain caused by elastic Poisson's ratio  $\nu_e$ , the other part is due to dilation effect of microcracking associated with cracking Poisson's ratio  $\nu_{cr}$ , which is of paramount significance in our model as can be seen in later sections.

### 3. Model establishment

It is known that concrete cylinder specimen under pure compression will undergo numerous parallel cracks development in the direction of loading. By studying the interior of concrete specimen that were loaded up to a certain level and then were subsequently unloaded (Slate *et al.*

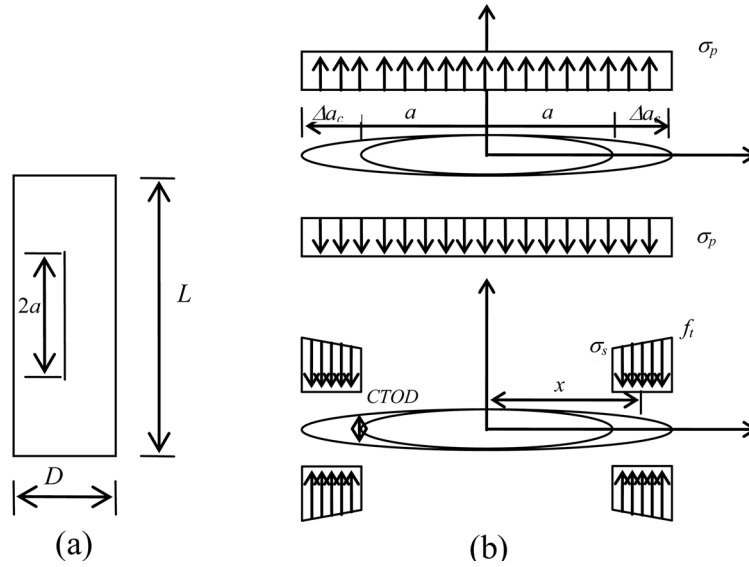


Fig. 3(a) The boundary condition, (b) The size of fracture process zone

1984), it was found that energy dissipation in the pre-peak regime was a global continuum-dominated process that may be attributed to microcracking throughout the entire specimen. So in this context, microcracks within the body were not treated as separate material discontinuities, but one principle crack in the loading direction as shown in Fig. 3(a). It was also assumed that the crack opening displacement was equal to the dilatation deformation in the transverse direction caused by cracking Poisson’s ratio  $\nu_{cr}$ .

With above assumptions, a major crack would develop with length  $2a$  in the central part of a compressive specimen as shown in Fig. 3(b). The stress intensity factor at the tip of crack caused by this deformation is (Murakami 1987)

$$K_I = \sigma_p \sqrt{\pi a} F_I \left( \frac{2a}{L}, \frac{2D}{L} \right) \tag{6}$$

However, since there was no physical tensile stress acting in the transverse direction of a compressive specimen,  $\sigma_p$  was introduced as a virtual stress associated with the deformation normal to crack length.  $F_I((2a/L), (2D/L))$ , the boundary correction factor, was a function relevant to the specimen geometrical condition. When  $2D=L$ , and the ratio  $2a/L$  was smaller enough,  $F_I((2a/L), (2D/L))$  could be approximately treated as 1. Then the stress intensity factor from Eq. (6) would be reduced to  $K_I = \sigma_p \sqrt{\pi a}$  same as the central crack with uniformly distributed average stress  $\sigma_p$ . The propagation of crack  $2a$  due to the deformation normal to crack could be regarded as the same crack under uniform average stress  $\sigma_p$  as shown in Fig. 3(b).

Pre-critical stable crack growth in heterogeneous materials is indeed encountered before the peak load is achieved. It is the existence of sub-critical extension of crack that deters the direct application of LEFM. Here we consider the elastic crack length  $2a$  plus the fracture process zone  $2\Delta a_c$ , which compose the effective crack length  $2a + 2\Delta a_c$  as shown in Fig. 3(b). The FPZ (fracture process zone) carries the cohesive force  $\sigma$  which tends to close the crack. FPZ is the identifiable region where microcracking occurs for cementitious materials. The combination of external force

and the cohesive force ameliorates the singularity at the crack tip predicted by LEFM, since infinite stress cannot actually develop in real materials. Similar to Dugdale approach, the size of the FPZ can be roughly estimated based on equilibrium condition

$$K_I^p + K_I^\sigma = 0 \quad (7)$$

where  $K_I^p$   $K_I^\sigma$  are the stress intensity factor due to external force and the cohesive force, respectively. For a center crack  $2a$  subjected to tensile load  $\sigma_p$ , the stress intensity factor can be expressed using

$$K_I^p = \sigma_p \sqrt{\pi(a + \Delta a_c)} = \sigma_p \sqrt{\pi a_c} \quad (8)$$

While for the stress intensity factor caused by cohesive force  $\sigma$ , superposition is utilized based on the center crack subjected to unit wedge force, which yields

$$K_I^\sigma = -\frac{1}{\sqrt{\pi a_c}} \int_a^{a_c} \sigma \left[ \sqrt{\frac{a_c+x}{a_c-x}} + \sqrt{\frac{a_c-x}{a_c+x}} \right] dx \quad (9)$$

Note the negative sign in the above equation is due to the fact that contribution of cohesive forces is to close the crack. For yielding type of materials, the closing stress is assumed to be a constant, namely, the yielding stress. While for the quasi-brittle materials, the cohesive forces existing in the FPZ is a unique function of the crack opening. Here, the cohesive stress distribution along the crack extension  $\Delta a_c$  is assumed to be linear as shown in Fig. 3(b), where  $\sigma_s$  is the stress at the point  $x=a$ . This is expressed as (Xu 1999).

$$\sigma = \sigma_s + (f_t - \sigma_s) \frac{x-a}{a_c - a} \quad (10)$$

Substitution of Eq. (10) into Eq. (9) gives

$$K_I^\sigma = -2 \sqrt{\frac{a_c}{\pi}} f_t \left\{ \frac{\pi}{2} \left( 1 - \frac{1 - \sigma_s/f_t}{1 - a/a_c} \right) - \left[ \arcsin \frac{a}{a_c} \left( \sigma_s/f_t - \frac{1 - \sigma_s/f_t}{1 - a/a_c} \right) - \frac{1 - \sigma_s/f_t}{1 - a/a_c} \sqrt{1 - \left( \frac{a}{a_c} \right)^2} \right] \right\} \quad (11)$$

Substituting Eqs. (8) and (11) and considering  $K_I = \sigma_p \sqrt{\pi a_c}$ , the equilibrium condition in Eq. (7) is in the form after some computations

$$\left( \frac{\sigma_s}{f_t} - \frac{1 - \sigma_s/f_t}{1 - a/a_c} \right) \frac{a}{a_c} = \frac{\pi}{2} \left( 1 - \frac{1 - \sigma_s/f_t}{1 - a/a_c} \right) - \frac{\sigma_p \pi}{2 f_t} + \frac{1 - \sigma_s/f_t}{1 - a/a_c} \sqrt{1 - \left( \frac{a}{a_c} \right)^2} \quad (12)$$

if  $a \rightarrow 0$ , then we could arrive at the approximate expression  $a_c$

$$\sqrt{a_c} = \frac{K_I/2f_t}{1 + \frac{\sigma_s}{f_t} \left( \frac{\pi}{2} - 1 \right)} \quad (13)$$

It is noted that if  $\sigma_s = f_t$  is regarded as the yielding limits, then Eq. (13) is recovered to the size of plastic zone predicted by Dugdale.

For the case of crack as shown in Fig. 3(b), the crack opening displacement at location  $x=a$  is approximately given by

$$CTOD = \frac{4\sigma_p}{E} \sqrt{2a_c \Delta a_c} \xrightarrow{a \rightarrow 0} \frac{4\sigma_p a_c}{E} \sqrt{2} \quad (14)$$

Substitution Eq. (13) into Eq. (14) results in

$$CTOD = \frac{2\sqrt{2}K_f^2}{f_t E \left[ 1 + \frac{\sigma_s}{f_t} \left( \frac{\pi}{2} - 1 \right) \right]} \quad (15)$$

$\sigma_s$  the stress at position where the crack opening displacement is equal to  $CTOD$ , can be estimated according to tension softening relationship proposed by Reinhardt *et al.* (Reinhardt 1986) that is widely used in both numerical and analytical analyses by many researchers

$$\sigma = f_t \left\{ \left[ 1 + \left( c_1 \frac{w}{w_0} \right)^3 \right] \exp \left( -c_2 \frac{w}{w_0} \right) - \frac{w}{w_0} (1 + c_1^3) \exp(-c_2) \right\} \quad (16)$$

where, the coefficients  $c_1$  and  $c_2$  are assumed to be material constants. For normal concrete, the three parameters in Eq. (16) were determined as  $c_1=3$ ,  $c_2=6.93$ ,  $w_0=160 \mu\text{m}$  according to the testing data using a fitting process.

When the stress intensity factor at the tip of the effective crack length has the value of  $K_{Ic}$ , unstable crack propagation occurs. At this critical state,  $CTOD$  simultaneously attaches its critical value termed as  $CTOD_c$ . For a known value of  $CTOD_c$ , the normalized stress  $\sigma_s/f_t$  at location with the crack opening displacement being  $CTOD_c$  and the total FPZ length  $2a_c$  at onset of unstable crack development will be derived following from relations Eqs. (13) and (14) as

$$2a_c = \frac{\sqrt{\pi} CTOD_c E}{4\sqrt{2} f_t} \frac{1}{1 + \frac{\sigma_s}{f_t} \left( \frac{\pi}{2} - 1 \right)} \quad (17)$$

Furthermore, the critical stress intensity factor for model I fracture pattern could be obtained from Eq. (13).

The determination of  $CTOD_c$  is based on the assumption that the dilation deformation in the lateral direction is intimately associated with microcracking

$$CTOD_c = D(\varepsilon_{un} v_{un} - \varepsilon_{un} v_e) = D \varepsilon_{un} v_{cr} \quad (18)$$

where  $D$  is the diameter of the cylinder specimen.

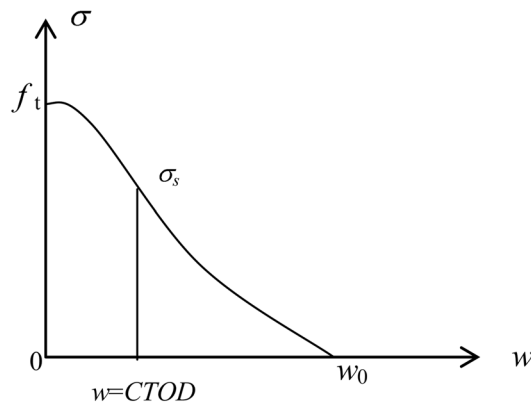


Fig. 4 The typical softening traction-separation curve

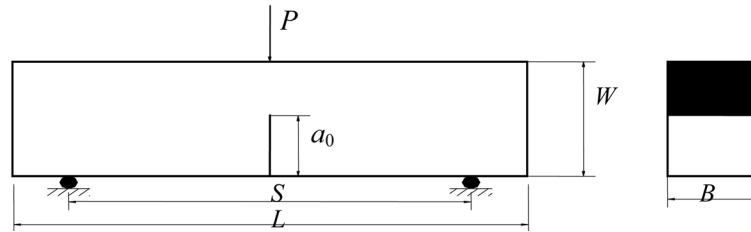


Fig. 5 The configuration of three-point bend notched beam

The procedures for obtaining  $K_{IC}^C$  are as follows: 1. obtain the crack Poisson's ratio from experimental stress-volumetric strain curves; 2. calculate the dilatation of the cylinder specimen due to crack Poisson's ratio and treat it as CTODc; 3. determine  $\sigma_s$  and  $f_i$ ; and 4. Calculate  $K_{IC}^C$  with Eq. (11).

#### 4. Preparation of specimens and setup

It was known that the larger the aspect ratio, the less effect from the boundary friction between the machine steel platens and the specimens' ends. The restraint effect could be viewed to die out at a distance equal to the specimen diameter according to the St.Venant's principal. So the slenderness  $L/D=3$  was particularly chosen here to gain the purely uniaxial compression in the specimens' central part. And at the same time the specimen should not be too long to cause buckling of the specimens. Bearing these in mind, the concrete cylinder specimens used in this investigation were 100 mm in diameter and 300 mm in height. To obtain the Poisson's ratio from Eq. (4), deformation in the longitudinal and circumferential direction should be measured simultaneously. Two axial extensometers (MTS 632.94F-20) with gage length 100 mm for axial strain measurements were attached to diametrically opposite sides at midheight of the specimens. While the change in circumference was measured by one circumferential extensometer (MTS 632.11F-20) with gauge length 3.75 mm mounted to the specimen by rollers. This is somewhat different from the traditional method to determine the transverse strain where the averaged value is taken over several strain gauges. The strain in periphery was actually the average over the entire material inside the circumference, thus more accurate in depicting the global crack propagation. To determine the modulus of elasticity, standard method of test in accordance with the recommendation of ASTM C469-94 (ASTM 1997) was carried out on an MTS 4600KN close-loop system, during which three main parameters were acquired continuously: the axial stress, the axial strain and the circumferential deformation.

To verify the soundness of the new method proposed, conventional notched three-point bending beam with same concrete were also prepared and tested. The fracture toughness was obtained using TPFM and DKM. The standard three-point bending notched beams were cast according to recommendation by RILEM (1990): width( $B$ )  $\times$  depth( $W$ )  $\times$  length( $L$ ) = 76 mm  $\times$  150 mm  $\times$  711 mm, with loading-span( $S$ ) to depth( $W$ ) ratio equal to 4 and the pre-cast notch length  $a_0$  to depth ratio 0.3(as shown in Fig. 5). The  $CMOD$  (crack mouth opening displacement) and the applied concentrated load  $P$  in the midspan were recorded continuously during the tests, where the  $CMOD$  was measured by means of a clip gauge glued on the surface in the middle of beam. The specimen was loaded progressively until unloading-reloading cycle at about 95% of the peak load in the post-

Table 1 Details of mix propositions

Concrete Designation	Binder			Water	Sand	Gravel	Superplasticiser KFDN
	Cement	SF	BFSG				
C30	1			0.55	2	2.7	
C60	1			0.4	1.7	2.5	0.4%
C80	0.9	0.1		0.3	1	1.8	0.8%
C90	0.5	0.1	0.4	0.23	1.2	1.8	2%

Note: SF=silica fume; BFSG=blast furnace slag. Superplasticiser was used by weight of binder (Cemnet+SF+BFSG)

peak process to get the unloading compliance according to TPFM. All the three-point bending beams were tested with an MTS machine of 250 KN capacity.

The aim of investigation was to make comparison between the proposed model and the conventional methods for different mix-propositions, ranging in target compressive strength from about 30 MPa to nearly 90 MPa. The details of the mix propositions used for preparing these specimens above were shown in Table 1.

Moulds were removed 24±5 hr after casting and left in curing room until tests at 28 days. At least three identical specimens were tested for both cylinder and three-point bending beam for the sake of reliability.

## 5. Analysis of test results

### 5.1 Cylinder tests

Fig. 6 presented typical stress-strain relationships for the different concrete composition in the present study, including stress( $\sigma$ )-axial strain( $\varepsilon_L$ ), stress( $\sigma$ )-circumferential strain( $\varepsilon_C$ ) and stress( $\sigma$ )-volumetric strain( $\varepsilon_V$ ). Table 2 gives the summarized test data and the calculated equivalent fracture toughness. The initial modulus of elasticity  $E_0$  was determined by the slope of fitting curve of linear portion of stress-axial strain curve. The  $\nu_e$  and  $\nu_{in}$  were used to designate the simultaneous strain ratio between the circumferential and the axial direction at the time when crack initiation and strain localization occurrence.

### 5.2 Beam tests

Three-point bending beams cast from the same batch of concrete used in cylinder tests were employed to find the conventional fracture toughness  $K_{IC}$ . In the present investigation, TPFM and DKM were used to extract the fracture toughness assigned to different superscripts  $K_{IC}^T$  and  $K_{IC}^D$  respectively. Fig. 7 illustrated a typical load-CMOD response of the beam. For TPFM proposed recommendation, the critical load  $P_{max}$ , the initial compliance  $C_i$  and the unloading compliance  $C_u$  from the load vs. CMOD curve were monitored during the tests for determination of  $K_{IC}^T$ , wherein the initial compliance was calculated by drawing a line from the origin to the load level about 1/3 the peak load. Unfortunately, the unloading compliances  $C_u$  for B80-3, B90-2 and B90-3 were not available because of the unsuccessful control, in this case, the unloading compliance was taken as

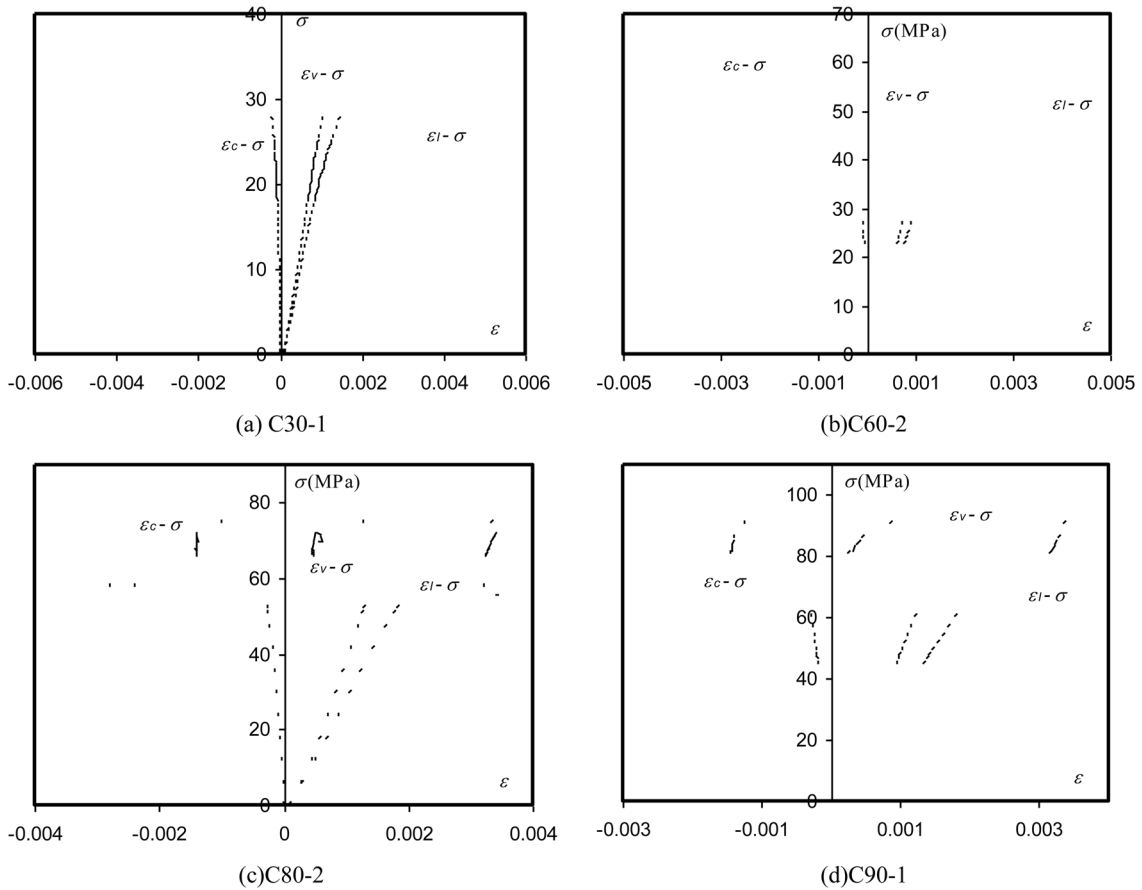


Fig. 6 Stress vs deformation curves for concrete cylinder under uniaxial compression

$C_u^*$  based on the directly recorded load-carrying capacity  $P_{max}$  and the corresponding  $CMOD_c$ . While for the DKM model, only the peak load  $P_{max}$  and its corresponding  $CMOD_c$  are needed for the calculation of  $K_{IC}^D$ . Details could be found in the relevant literature (Shah 1991, Xu 1999). The measured data together with the calculated results are summarized in Table 3.

### 5.3 Data analysis

It is now commonly accepted that the fracture toughness derived from the nonlinear elastic fracture mechanics should be material property that is independent on the specimen size as well as specimen geometry, as substantiated by many experimental and calculation results in the literature. If we plot the fracture toughness  $K_{IC}^C$  obtained from concrete cylinders and  $K_{IC}^T$ ,  $K_{IC}^D$  from three-point bending beams against compressive strength in Fig. 8, we can find their values are very close, at least in acceptable and reasonable range. Fracture toughness increases with increasing compressive strength, but not in a linear manner as some researchers pointed out. Comparing to the strengths increase, the increase of  $K_{IC}$  is within a much smaller percentage. A simple mathematical explanation is as follows: the relationship between fracture toughness and compressive strength in Fig. 8 can be

Table 2 Results from test data for different strength concrete

Specimen	$\varepsilon_1(10^{-6})$	$\sigma_1$ (MPa)	$E_0$ (Gpa)	$\varepsilon_{un}/\varepsilon_1$	$\sigma_{un}/\sigma_1$	$\nu_{cr}$	$f_i$ (MPa)	CTOD <sub>c</sub> (m×10 <sup>-6</sup> )	$\sigma_s/f_i$	$2a_c$ (mm)	$K_{IC}^C$ (MPam <sup>1/2</sup> )
C30-1	2795.0	35.61	25.37	0.740	0.946	0.136	3.39	28.14	0.334	16.393	1.009
C30-2	2694.3	37.62	26.08	0.743	0.939	0.148	3.48	29.52	0.321	16.839	1.058
C30-3	3119.0	32.59	22.81	0.642	0.917	0.147	3.24	29.44	0.321	16.952	0.954
Ave.	2869.4	35.27	24.75	0.708	0.934	0.144	3.37	29.03	0.33	16.728	1.007
C60-1	2941.1	59.10	30.64	0.812	0.946	0.112	4.36	26.80	0.348	11.285	1.232
C60-2	2817.0	59.56	30.69	0.858	0.959	0.107	4.38	25.87	0.359	10.772	1.217
C60-3	2894.2	59.04	30.11	0.983	0.999	0.100	4.36	28.36	0.332	11.840	1.251
Ave.	2884.1	59.23	30.48	0.884	0.968	0.106	4.37	27.01	0.35	11.299	1.233
C80-1	3174.1	80.33	31.34	0.970	0.989	0.087	5.08	26.87	0.348	8.519	1.347
C80-2	3272.0	80.35	30.66	0.912	0.971	0.094	5.09	28.09	0.335	8.762	1.358
C80-3	3016.9	77.21	31.75	0.981	0.997	0.087	4.98	25.79	0.360	8.564	1.319
Ave.	3154.3	79.30	31.25	0.954	0.986	0.090	5.05	26.92	0.35	8.615	1.341
C90-1	3262.3	95.74	36.11	0.901	0.955	0.083	5.55	24.31	0.378	7.346	1.447
C90-2	3487.1	101.71	38.05	0.890	0.961	0.082	5.72	25.35	0.365	3.820	1.535
C90-3	3394.7	95.06	35.39	0.915	0.968	0.086	5.53	26.79	0.348	4.050	1.491
C90-4	3357.5	96.15	35.85	0.916	0.968	0.099	5.56	30.32	0.313	4.670	1.588
Ave.	3375.4	97.16	36.350	0.905	0.963	0.087	5.591	26.694	0.351	8.106	1.515

Note the stress involved was expressed as a fraction of the ultimate strength  $\sigma_1$ , referred as the  $y = \sigma/\sigma_1$ , similarly the strain can be denoted with the symbol  $x = \sigma/\varepsilon_1$ , where  $\varepsilon_1$  is axial strain corresponding to the strength  $\sigma_1$ . No direct tension strength  $f_t$  is obtained here, so the empirical formula  $f_t = 0.54\sqrt{f_c}MPa$  (Ghosh 1987) is used. Also we should know that  $f_c$  is the compressive strength for cylinder specimen with  $L/D = 2$ , regarding the specimen in the experiments with  $l/d = 3$ , a correction factor should be considered, that is  $\sigma_1 = 0.94f_c$ .

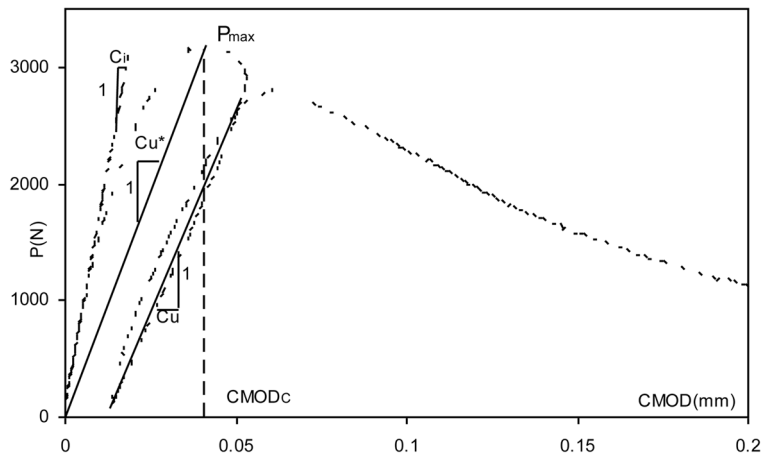


Fig. 7 Test record for specimen B30-3 load versus CMOD

expressed by a logarithmic function  $K_{Ic} = kLn(f_c) + m$ , so the increase rate of fracture toughness  $dK_{Ic} = (k/f_c)df_c$  is obviously decreasing along with the compressive strength increasing rate. Although increasing fracture toughness means a higher resistance to cracking, the material behaviors

Table 3 Measured test data

	$C_i \times 10^{-6}$ (mm/N)	$C_u \times 10^{-6}$ (mm/N)	$P_{max}(N)$	$CMOD \times 10^{-3}$ (mm)	$a_c/w$ (TPFM)	$a_c/w$ (DKM)	$K_{IC}^T$ (MPam <sup>1/2</sup> )	$K_{IC}^D$ (MPam <sup>1/2</sup> )
C30	611×150×76 mm		$a_0/w=0.3$	$H_0=1.73$ mm	$f_c=35.27$ MPa			
B30-1	7.32	17.27	3533.13	49.49	0.493	0.454	1.304	1.162
B30-2	6.94	14.78	3191.90	41.17	0.474	0.448	1.116	1.034
B30-3	7.22	14.14	2919.60	42.14	0.458	0.462	0.977	0.989
Ave.							1.132	1.061
C60	611×150×76 mm		$a_0/w=0.3$	$H_0=1.73$ mm	$f_c=59.23$ MPa			
B60-1	6.59	14.30	3461.61	50.41	0.483	0.481	1.243	1.235
B60-2	5.97	14.70	3365.96	47.58	0.506	0.493	1.300	1.248
B60-3	5.55	13.57	3253.08	44.67	0.499	0.501	1.230	1.238
B60-4	5.97	12.16	3677.04	48.14	0.465	0.479	1.248	1.302
B60-5	5.80	12.93	3766.66	44.19	0.482	0.464	1.346	1.274
Ave.							1.273	1.260
C80	611×150×72 mm		$a_0/w=0.3$	$H_0=1.73$ mm	$f_c=79.3$ MPa			
B80-1	6.78	9.48	3844.21	49.82	0.436	0.464	1.261	1.372
B80-2	6.66	10.73	4015.69	45.47	0.449	0.442	1.369	1.341
B80-3	6.50	14.11	3554.68	50.17	0.487	0.487	1.361	1.361
Ave.							1.330	1.358
C90	611×150×76 mm		$a_0/w=0.3$	$H_0=1.73$ mm	$f_c=97.16$ MPa			
B90-1	5.42	8.23	5471.12	40.28	0.407	0.389	1.555	1.479
B90-2	5.43	7.79*	5428.03	42.31	0.399	0.399	1.509	1.509
B90-3	5.44	6.86*	5805.46	39.85	0.375	0.375	1.510	1.510
Ave.							1.525	1.499

Note  $f_c$  is the mean ultimate strength from concrete cylinder of the same composition;  $H_0$  is the clip gauge holder thickness

more brittle.

From the experimental results for concrete of different strength under uniaxial compressive (Fig. 6 and Table 2), it is found the stress-strain relations are strongly influenced by the compressive strength: the higher the compressive strength, the longer portion of linear part of stress-strain curve. This is one characteristic of much more brittleness of higher strength concrete, partially due to the improvement in the interfacial transition zone (ITZ) by the reduction of  $w/c$  ratio and the addition of silica fume, which can fill large pores and consume calcium hydroxide in ITZ.

Another interesting thing concluded from Table 2 is decreasing values of  $CTOD_c$  along with the increasing compressive strength, meaning a smaller amount of cracking occurs in such higher strength concrete than in the normal strength concrete, and this point is touched in reference (Smadi *et al.* 1989).

The Poisson's ratio is one essential parameter in the proposed model. Actually it increases against the strain increase, indicating the dilation effect caused by the growth of microcracks. With help of it, it confirmed the fact that the tensile behavior is still the vital factor governing the failure of

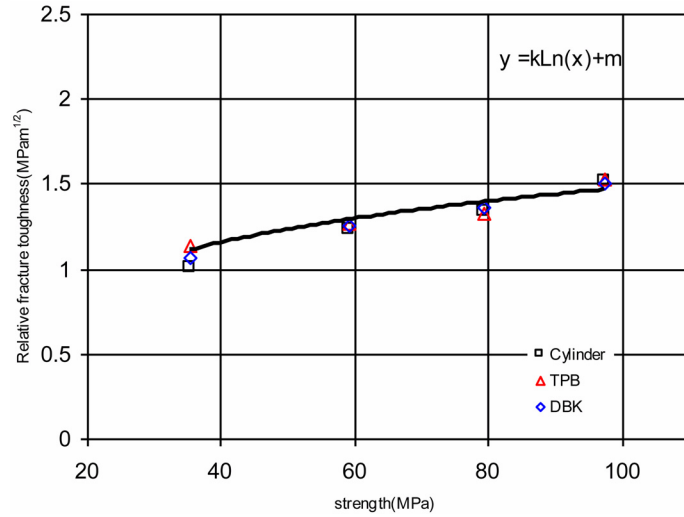


Fig. 8 Comparison of relative fracture toughness of uniaxial compression tests with those obtained from three-point bend beams

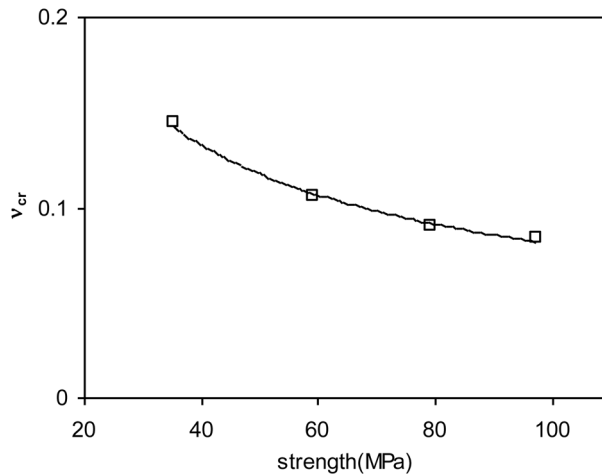


Fig. 9 Cracking Poisson's ratio and compressive strength

concrete. It is evaluated as the ratio between the circumferential strain and the longitudinal strain, something different from the conventional method where the averaged diametrical strain was used to find transverse strain. Though these two methods should produce the same  $\nu$  in theory, actually the results are beyond our expectations: the calculated results in Table 2 are not identical as commonly accepted elastic Poisson's ratio. It would not be surprising if we consider the fact that concrete material itself is inhomogenous. The traditional method to find  $\nu$  is based on the average value measured by strain gauge clipped at several locations around the periphery of specimen, as can be viewed as a local fracture behavior of concrete specimen. While the transverse strain presented in this paper is measured by the circumferential strain, which is a global strain measurement comparing the local measurement in the formal method. This is more reasonable to

characteristic the global fracture behavior of concrete. The cracking Poisson's ratio  $\nu_{cr}$ , discrepancy between the Poisson's ratio  $\nu_{un}$  at the onset of unstable crack propagation and the elastic Poisson's ratio  $\nu_e$ , plays a pivotal role in the determination of fracture toughness  $K_{IC}^C$ . It tends to decrease with the increasing compressive strength as indicated by Fig. 9, meaning somewhat smaller lateral deformation developed for higher strength concrete during crack stable propagation, and it can be proposed to characterize the brittleness of concrete.

## 6. Conclusions

The fracture properties of concrete have been studied by employing the uniaxial compressive concrete cylinder specimen with aspect ratio of 3. The research presented supports the following conclusions:

1. The non-linear stress-strain behavior of concrete at monotonic uniaxial compression implies that concrete experience progressive microcrack growth prior the attainment of the ultimate failure. The formation and propagation of microcracks are responsible for the fracture of concrete under uniaxial compression something same as in the failure of concrete under tension.

2. The cracking Poisson's ratio  $\nu_{cr}$  plays an important role in the determination of concrete specimen failure under uniaxial compression. It can be treated as a damage parameter in describing the failure progress of concrete under uniaxial compression.

3. By utilizing  $\nu_{cr}$ , the dilatation deformation of a concrete cylinder under compression can be calculated and treated as crack opening displacement.

4. Interpretation of fracture toughness using the newly introduced method based on a concrete cylinder under compression is feasible and the results agree well with the results of conventional three-point bending test.

5. Because the new method is simple and straightforward in both experiment and calculation, there is a good potential for its application in civil engineering.

## Acknowledgements

The support from China Ministry of Science and Technology under grant of 2009CB623200 is gratefully acknowledged.

## References

- ASTM (1997) "Standard test method for static modulus of elasticity and Poisson's ratio of concrete in compression", *Annual Book of ASTM Standards*, ASTM, Philadelphia, **4**(2), 238-241.
- Asferg, J.L, Poulsen, P.N and Nielsen, L.O. (2007), "A direct XFEM formulation for modeling of cohesive crack growth in concrete", *Comput. Concrete*, **4**(2), 83-100.
- Bazant, Z.P. and Kazemi, M.T. (1990), "Determination of fracture energy, process zone length and brittleness number from size effect, with application to rock and concrete", *Int. J. Fracture*, **44**, 111-131.
- Bazant, Z.P. and Oh, B.H. (1983), "Crack band theory for fracture of concrete", *Mater. Struct.*, RILEM, **16**, 155-177.
- Carpeteri, A., Ferro, G. and Monetto, I. (1999), "Scale effects in uniaxially compressed concrete specimens",

- Mag. Concrete Res.*, **51**, 217-225.
- Choi, S.W. and Shah, S.P. (1998), "Fracture mechanism in cement-based materials subjected to compression", *J. Eng. Mech.- ASCE*, **124**(1), 94-102.
- Dujic, J., Brank, B., Ibrahimovic, A. and Brancherie, D. (2010), "An embedded crack model for failure analysis of concrete solids", *Comput. Concrete*, **7**(4).
- Ghosh, S.K. (1997), "Provisions in U.S. codes related to high-strength concrete", *High Strength Concrete, First International Conference*, 568-581.
- Hillerborg, A. (1976), "Analysis of crack formation and crack growth in concrete by means of fracture mechanics and finite elements", *Cement Concrete Res.*, **6**, 773-782.
- Hillerborg, A. (1985), "The theoretical basis of method to determine the fracture energy  $G_F$  of concrete", *Mater. Struct.*, **18**(106), 291-296.
- Horii, H. and Nemat-Nasser, S. (1986), "Brittle failure in compression: splitting, faulting, and brittle-ductile transition", *Philosophical Transactions Royal Soc. London: Series A Math. Phys. Sci.*, **319**(1549), 337-374.
- Jansen DC, Shah, SP, and Rossow, EC (1995), "Stress-strain results of concrete from circumferential strain feedback-control testing", *ACI Mater. J.*, **92**(4), 419-428.
- Jenq, Y.S. and Shah, S.P. (1985a), "Two parameter fracture model for concrete", *J. Eng. Mech., ASCE*, **111**(10), 1227-1241.
- Jenq, Y.S. and Shah, S.P. (1985b), "A fracture toughness criterion for concrete", *Eng. Fracture Mech.*, **21**(5), 1055-1069.
- Lee, Y.H. and Willam, K. (1997), "Mechanical properties of concrete in uniaxial compression", *ACI Mater. J.*, **94**(6), 457-471.
- Murakami, Y. (1987), "Stress intensity factors handbook", *Pergamon Press*, **1**, 71-72.
- Neville, A.M. (2002), *Properties of concrete*, Fourth and Final Edition Standards updated to 2002, Pearson Education Limited.
- Rasko, P., Ojdrovic, S.M. and Henry, J.P. (1987), "Fracture behavior of notched concrete cylinder", *J. Eng. Mech.*, **113**(10), 1551-1564.
- Reinhardt, H.W., Cornelissen, H.A.W. and Hordijk, D.A. (1986), "Tensile tests and failure analysis of concrete", *J. Struct. Eng.*, **112**(11), 2462-2477.
- RILEM Recommendations (1990), "Determination of fracture parameters of plain concrete using three-point bend tests", *Mater. Struct.*, **23**, 457-460.
- Shah, S.P., Swartz, S.E. and Ouyang, C. (1995), *Fracture mechanics of concrete: application of fracture mechanics to concrete, rock and other quasi-brittle materials*, New York, Willey.
- Shah, S.P. and Carpinteri, A. (1991), *Fracture mechanics test methods for concrete*, Chapman And Hall.
- Shah, S.P. and Chandra, S. (1968), "Critical stress, volume change and microcracking of concrete", *ACI J.*, **65**(9), 770-781.
- Slate, F.O. and Hover, K.C. (1984), "Microcracking in concrete, fracture mechanics of concrete", *Martinus Nijhoff Publisher, The Hague*, 137-159.
- Smadi, M.M. and Slate, F.O. (1989), "Microcracking of high and normal strength concretes under short- and long- term loadings", *ACI Mater. J.* **86**(2), 117-127.
- Su, E.C.M. and Hsu, Thomas T.C. (1988), "Biaxial compression fatigue and discontinuity of concrete", *ACI Mater. J.*, **85**(3), 178-188.
- Van Mier, J.G.M. (1986), "Multiaxial strain-softening of concrete, Part I: fracture", *Mater. Struct.*, **19**(111), 179-190.
- Xu, Shilang and Reinhardt, H.W. (1998), "Crack extension resistance and fracture properties of quasi-brittle softening materials like concrete based on the complete process of fracture", *Int. J. Fracture*, **92**, 71-99.
- Xu, Shilang and Reinhardt, H.W. (1999), "Determination of double-K criterion for crack propagation in quasi-brittle fracture, Part II: analytical evaluating and practical measuring methods for three-point bending notched beam", *Int. J. Fracture*, **98**, 51-177.
- Yin, W.S., Su, E.C.M., Mansur, M.A. and Hsu, T.T.C. (1989), "Biaxial tests of plain and fiber concrete", *ACI Mater. J.*, **86**(3), 236-243.
- Zhao, Y.H., Xu, S.L. and Li, Z.J. (2003), "An analytical and computational study on energy dissipation along fracture process zone in concrete", *Comput. Concrete*, **1**(1), 47-60.